International Journal of Heat and Mass Transfer 52 (2009) 3009–3023

Contents lists available at ScienceDirect

International Journal of Heat and Mass Transfer

journal homepage: www.elsevier.com/locate/ijhmt

Flow and heat transfer in a driven square cavity with double-sided oscillating lids in anti-phase

Dedy Zulhidayat Noor, P. Rajesh Kanna [1], Ming-Jyh Chern *

Department of Mechanical Engineering, National Taiwan University of Science and Technology, 43 Sec. 4 Keelung Road, Taipei 10607, Taiwan, ROC

ARTICLE INFO

Article history:
Received 30 January 2008
Received in revised form 24 October 2008
Accepted 23 January 2009
Available online 26 March 2009

Keywords:
Cavity flow
Oscillating lids
Vortex dynamics
Average Nusselt number

ABSTRACT

Flow and heat transfer inside a square cavity with double-sided oscillating lids have been studied numerically. The oscillating angular frequency of lid motion, ϖ, and Reynolds number, Re, are two important parameters in this study. In terms of primary vortices, simulations at Re and ϖ up to 1000 and 5, respectively, showed that the flow patterns can be categorized into four modes: (i) a pair of vertical vortices, (ii) a pair of swing vortices, (iii) diagonal-dominated vortices and (iv) two pairs of swing vortices. The flow patterns change at different frequencies for Reynolds numbers greater than 300. Nevertheless, the oscillating frequency did not offer significant effect to change flow pattern at very low Reynolds number such as at $Re \leqslant 10$. Heat transfer, represented by average Nusselt number (Nu) along the lids is increased at higher Re whereas it is decreased as ϖ increases.

1. Introduction

Lid-driven cavity flow is found in many engineering applications, for example, within mixing, coating and drying technologies. There are many numerical studies in classical single lid-driven cavity flow conducted by researchers and some of them can be found from Refs. [1–8]. Some studies of cavity flow with an oscillating lid have been done by few researchers [9–13]. Soh and Goodrich [9] introduced a new time-accurate finite difference method to solve unsteady incompressible Navier–Stokes equations in primitive variables. They solved flows inside a cavity with an impulsively starting lid and an oscillating lid at Re = 400 by using solution of lid-driven cavity flow with constant lid speed as an initial condition. Their results give a basic information of cavity flow with an oscillating lid. Iwatsu et al. [10] performed a numerical investigation to study the effect of external excitation on the flow structure in a square cavity. They found less variation of flow structures in low frequency values. Nishimura and Kunitsugu [11] studied fluid mixing and mass transfer in two-dimensional cavities with an oscillating lid. They used the Galerkin finite element method to solve cavity flow problems for different amplitudes of the oscillating wall velocity, Strouhal number and aspect ratio. The simulations have been performed at low Reynolds number equal to 50. It was shown that the mixing depends on an optimum oscillatory frequency, oscillating amplitude and aspect ratio. Sriram et al. [12] made analysis of variations and flow structures in a periodically lid-driven cavity at different frequencies, amplitudes and Reynolds numbers. It was found that at very low Re, the flow throughout the periodic driven cavity qualitatively resembles the classical steady lid-driven cavity flow. On the contrary, at high Re, the entire cavity is occupied with multiple vortices. Recently, Khanafer et al. [13] have performed numerical simulations to investigate the effects of a number of pertinent dimensionless parameters, namely the Reynolds number, Grashof number and the dimensionless oscillation frequency of the sliding lid on unsteady mixed convection in a driven cavity using an externally excited sliding lid.

The single lid-driven cavity flow problems were extended to the case of two-sided lid-driven cavity flow by some researchers [14–17]. Kuhlmann et al. [14] performed experimental and theoretical investigations for the two- and three-dimensional flows driven by anti-parallel motion of two facing walls. Their results indicated that the existence of non-unique two-dimensional steady flows depends upon the cavity aspect ratio and the Reynolds number. Albensoeder and Kuhlmann [15] studied the three-dimensional instability of two counter-rotating vortices in the cavity flow driven by two parallel moving walls with the same speed. They made numerical investigation about the type of instability and the dependence of the critical Reynolds and wave number on the aspect ratio. Furthermore Albensoeder and Kuhlmann [16] investigated the stability balloon for the double-lid-driven cavity flow. The flow is driven by the parallel or anti-parallel motion of two facing walls. When the cavity is infinitely extended in the spanwise directional variety of different three-dimensional flow instabilities can arise.

* Corresponding author. Tel.: +886 2 27376496; fax: +886 2 27376460.
E-mail address: mjchern@mail.ntust.edu.tw (M.-J. Chern).
[1] Present address: Department of Mechanical Engineering, Kalasalingam University, Anand nagar, Krishnankoil-626 190. (via). Srivilliputtur, Virudunagar Dist., Tamil Nadu, India.

0017-9310/$ - see front matter © 2009 Elsevier Ltd. All rights reserved.
doi:10.1016/j.ijheatmasstransfer.2009.01.037

Nomenclature

Re	Reynolds number, u_0H/υ
Gr	Grashof number, $g\beta(T_H - T_C)H_3/\upsilon^3$
Pr	Prandtl number, υ/α
Nu	average Nusselt number
C_f	friction coefficient
H	cavity height (m)
u_0	constant lid speed (m s^{-1})
T_H	temperature of the bottom lid (K)
T_C	temperature of the top lid (K)
g	gravitational acceleration (m s^{-2})
t	non-dimensional time
f	non-dimensional frequency
p	non-dimensional pressure
u	non-dimensional velocity component in the x-direction
v	non-dimensional velocity component in the y-direction
x, y	non-dimensional Cartesian coordinates
Greek symbols	
ϖ	non-dimensional oscillation angular frequency, $\omega H/u_0$
ω	oscillation angular frequency
θ	non-dimensional temperature
υ	kinematic viscosity of fluid (m^2 s^{-1})
α	thermal diffusivity (m^2 s^{-1})
β	coefficient of thermal expansion (K^{-1})

Luo and Yang [17] observed fluid flow and heat transfer in a two-sided lid-driven cavity with an aspect ratio of 1.96 numerically. The top and bottom lids of the cavity have different temperatures and move in opposite directions to generate a temperature gradient and thermal transport. The Reynolds number and the Grashof number are used as main parameters for the isothermal and the non-isothermal flow cases, respectively.

Among the studies of square cavity flows, we believe that there is no available manuscript about oscillatory double-sided lid-driven cavity flow. The present study is performed to observe this type of flow numerically. The dimensionless lid oscillating angular frequency, ϖ, together with Reynolds number are considered as two important parameters in this present study. The numerical scheme was validated with the cavity flow with oscillating lid of Khanafer et al. [13].

2. Problem description and numerical procedure

2.1. Problem description

A two-dimensional square cavity is considered for the present study as shown in Fig. 1. The top and bottom walls are considered as oscillating lids following the cosine function $u = u_0 \cos\omega t$ and $u = -u_0 \cos\omega t$, respectively, while the no-slip condition is imposed on the solid walls. The bottom wall is sustained at a higher temperature and the vertical walls are assumed to be adiabatic. The working fluid is air with constant Pr = 0.71. There are two important parameters in this study, i.e., Reynolds number, Re, and dimensionless oscillating angular frequency of lid motion, ϖ, defined as $\varpi = \omega H/u_0$ where ϖ, u_0 and H are lid oscillation frequency, maximum lid speed and cavity height, respectively. Re and ϖ vary from 10 to 1000 and from 1 to 5, respectively. Buoyancy effect was not considered except for validation.

2.2. The governing equations

The two-dimensional Navier–Stokes, continuity and energy equations in primitive variables for an unsteady incompressible laminar viscous flow with the Boussinesq assumption are denoted in dimensionless forms using the following dimensionless variables

$$x = \frac{x^*}{H} \quad y = \frac{y^*}{H} \quad u = \frac{u^*}{u_0} \quad v = \frac{v^*}{u_0} \quad \theta = \frac{T - T_C}{T_H - T_C}$$
$$p = \frac{p^*}{\rho u_0^2} \quad \mathrm{Re} = \frac{uH}{\upsilon} \quad \mathrm{Pr} = \frac{\upsilon}{\alpha} \quad \mathrm{Gr} = \frac{g\beta(T - T_C)H^3}{\upsilon^2} \tag{1}$$

Hence, the non-dimensional governing equations are continuity equation,

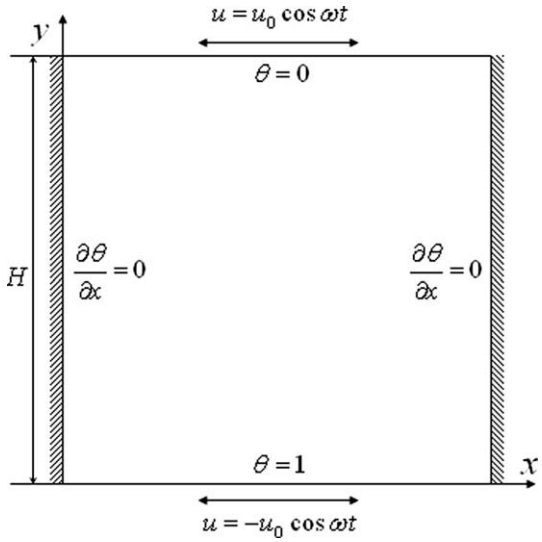

Fig. 1. Problem description and geometry of the square cavity.

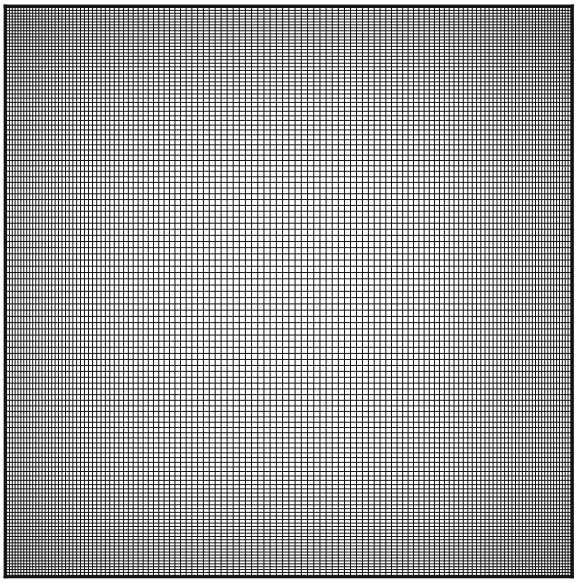

Fig. 2. The typical grid arrangement, 125 × 125 grid size.

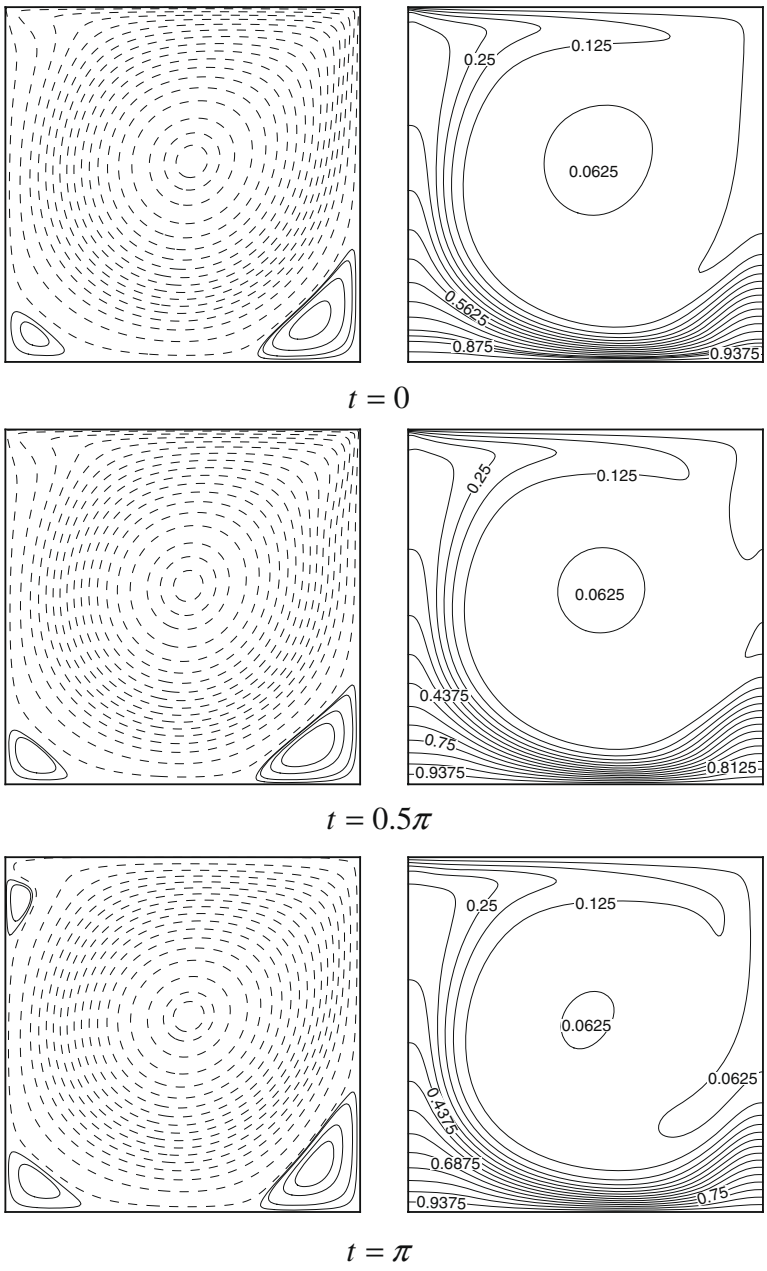

Fig. 3. Streamline (left) and isotherm (right) contours for Re = 1000, Gr = 100, $\varpi = 1$.

$$\frac{\partial u}{\partial x} + \frac{\partial v}{\partial y} = 0 \tag{2}$$

momentum equation,

$$\frac{\partial u}{\partial t} + u\frac{\partial u}{\partial x} + v\frac{\partial u}{\partial y} = -\frac{\partial p}{\partial x} + \frac{1}{\mathrm{Re}}\nabla^2 u \tag{3}$$

$$\frac{\partial v}{\partial t} + u\frac{\partial v}{\partial x} + v\frac{\partial v}{\partial y} = -\frac{\partial p}{\partial y} + \frac{1}{\mathrm{Re}}\nabla^2 v + \frac{\mathrm{Gr}}{\mathrm{Re}^2}\theta \tag{4}$$

energy equation,

$$\frac{\partial \theta}{\partial t} + u\frac{\partial \theta}{\partial x} + v\frac{\partial \theta}{\partial y} = \frac{\nabla^2 \theta}{\mathrm{RePr}} \tag{5}$$

where u, v, p and θ are the dimensionless variables of velocity components in the x- and the y-directions, pressure and temperature, respectively, Re, Gr and Pr are the Reynolds number, Grashof number and Prandtl number, respectively. The dimensionless average Nusselt number is determined along both the top and bottom walls using the formula,

$$\overline{Nu} = -\int_0^1 \frac{\partial \theta}{\partial y} dx \tag{6}$$

Also, the friction coefficient along the oscillating lids is given by,

$$C_f = \frac{2}{\mathrm{Re}}\frac{\partial u}{\partial y} \tag{7}$$

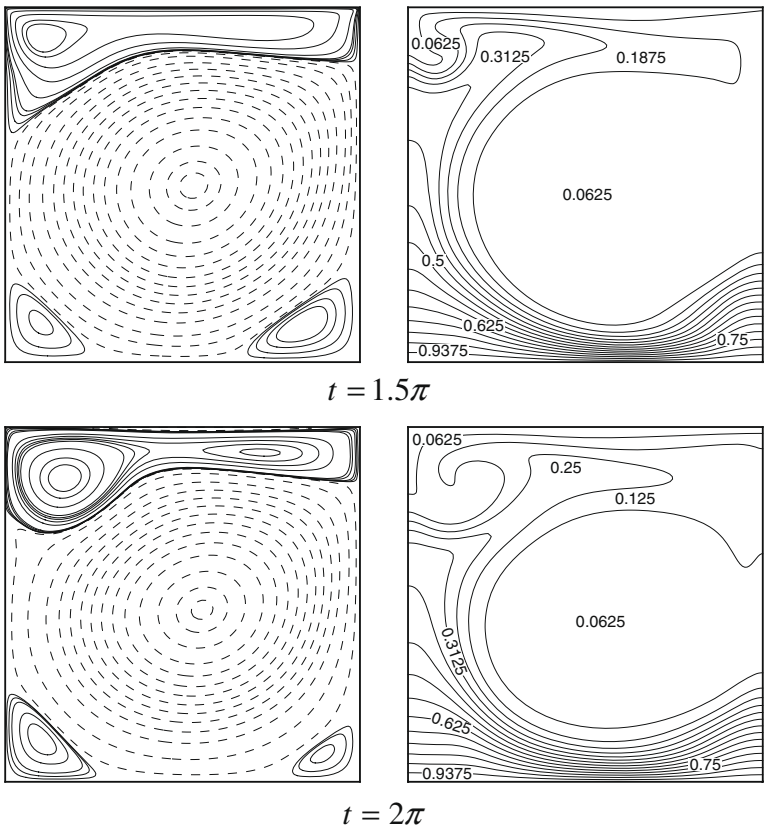

Fig. 3 (*continued*)

The diffusive terms of Eqs. (3) and (4) are discretised using the second-order central difference scheme while the convective terms are discretised using the quadratic upstream interpolation for convective kinetics (QUICK) scheme. The fourth-order Runge–Kutta method is used for the solution of the transient terms while the pressure terms are solved by using SOLA method [18].

The dimensionless time step of 10^{-3} was used and the mass residual criterion equal or less than 10^{-5} was employed at each time step in this work. We performed simulations for the lid motion at constant velocities ($u = u_0 = 1$ and $u = -u_0 = -1$ for top and bottom lids, respectively) till the steady solutions are reached using these results as the initial conditions of all simulations with the oscillating lids. The solutions should be identical at every cycle in the periodic state.

2.3. Validation of the in-house numerical code

Since there is no public data for flows inside a double-sided oscillating lid-driven cavity, the established numerical code was validated with the previous results with a single oscillating lid [13]. We performed a systematic grid refinement study, i.e., 75×75, 100×100, 125×125 and 150×150 grid to obtain the grid independent solution. Furthermore a 125×125 clustered grid with the smallest cells 0.0025 at the corner of the cavity and the biggest cell 0.015 at the center of the cavity are chosen for all simulations in the present study. The typical grid arrangement is shown in Fig. 2.

The simulation was done for Re, Gr and ϖ equal to 1000, 100 and 1, respectively, where the gravitation is in $-y$-direction. The streamline and isotherm contours during a period are presented in Fig. 3 while the variations of the average Nusselt number on the top and bottom wall are shown in Fig. 4. It is found that there is a good agreement between the present results and the previous study performed by Khanafer et al. [13].

3. Results and discussion

3.1. Flow patterns

According to the results obtained by the numerical model, it is found that the flow patterns, in terms of primary vortices, can be categorized into four modes: (i) a pair of vertical vortices, (ii) a pair of swing vortices, (iii) diagonal-dominated vortices and (iv) two pairs of swing vortices. It is noted that apart form the validation of the present numerical code buoyancy effect was not considered for all the cases in the present simulations. For all cases in the present study, about 18 cycles are required to reach the periodic state from the initial conditions. Furthermore, the conditions at the 19th cycle are taken as a typical solution for a period at each case in this present study. The periodic condition is represented by plot of time histories of u- and v-velocity as shown in Fig. 5.

3.1.1. A pair of vertical vortices

Jeong and Hussain [19] defined a vortex in an incompressible flow in terms of the eigenvalues of the symmetric tensor $S^2 + \Omega^2$, where S^2 and Ω^2 are the symmetric and antisymmetric parts of the velocity gradient ∇u_i, respectively. This definition is the underlying reason in representing the vortex core geometry correctly in unsteady low Re flows as occurs in our mode. This mode exists at a very low Reynolds number less than 10 and represented by flow patterns shown in Fig. 6. At $t = 0.25T$ and $t = 0.75T$, the lids are at rest instantaneously. After this time step, the direction of lid motion starts changing to the opposite side. The vortex core becomes

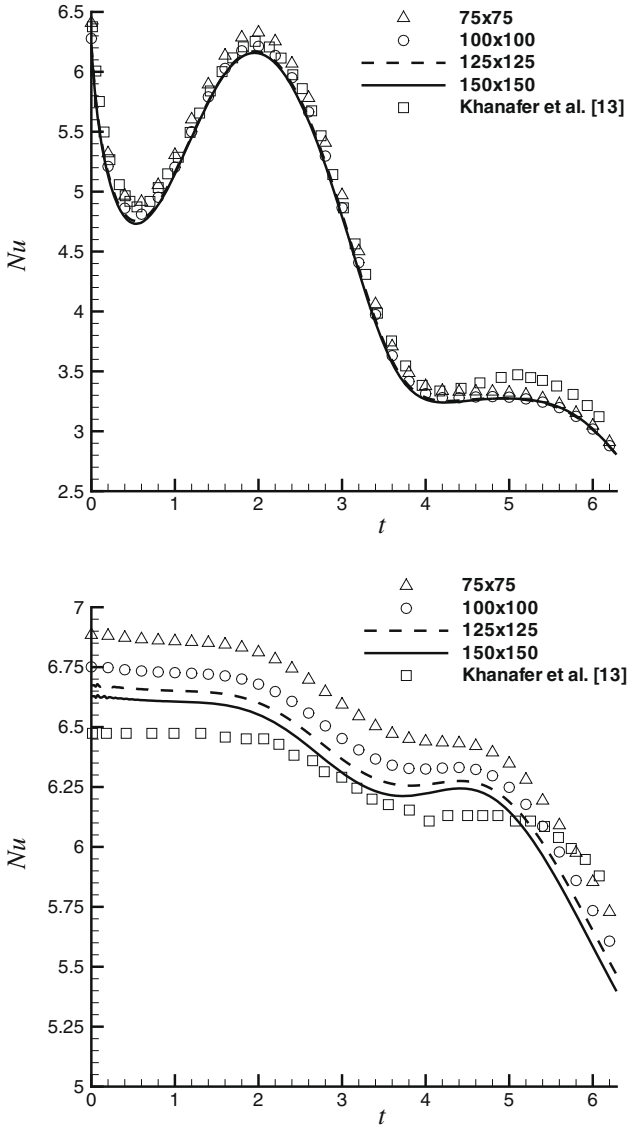

Fig. 4. The average Nusselt number for Re = 1000, Gr = 100, $\varpi = 1$ at $t = 0$. The top lid (upper) and the bottom lid (lower).

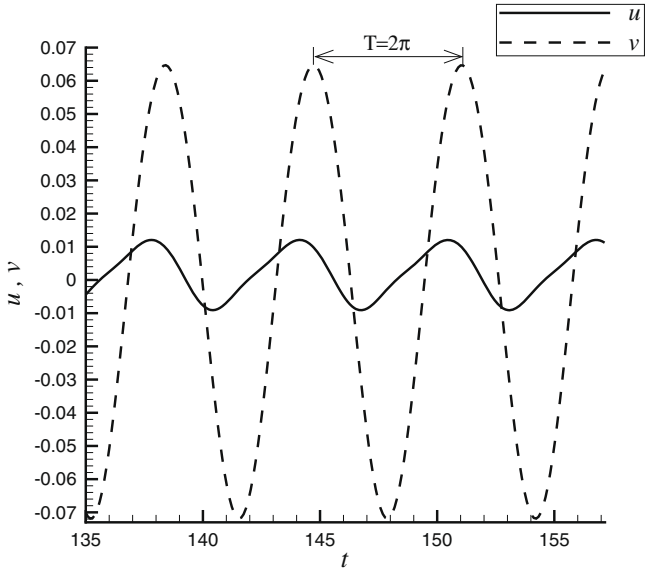

Fig. 5. Time history of u- and v-velocity at the center of the cavity.

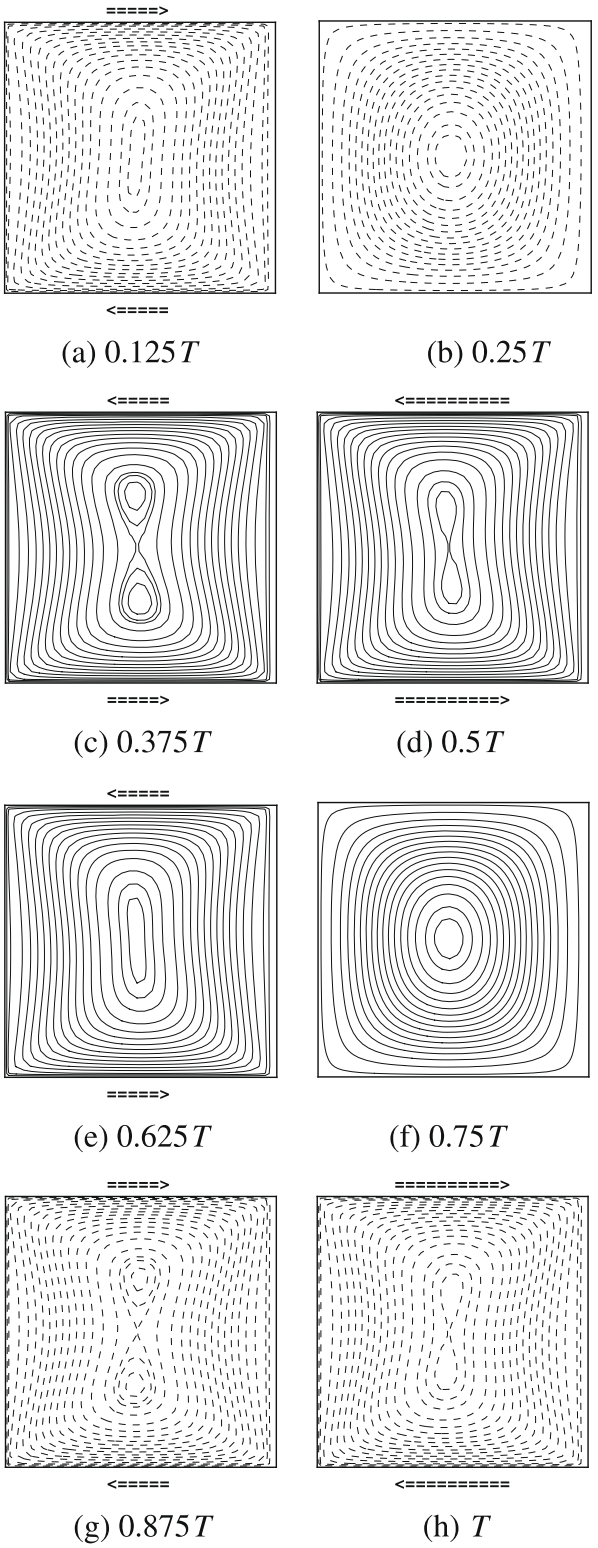

Fig. 6. Streamline contours during a period, Re = 10, $\varpi = 1$ (first mode).

elongated vertically and a small separatrix is forming during two parts of a single cycle. It becomes smaller and subsequently forms a single primary vortex at the center of cavity when the lids decelerated (Fig. 6c–f). The saddle point existed and located at the center of cavity. The streamline patterns are very similar during the two half cycles. There is a particular symmetry operation involving

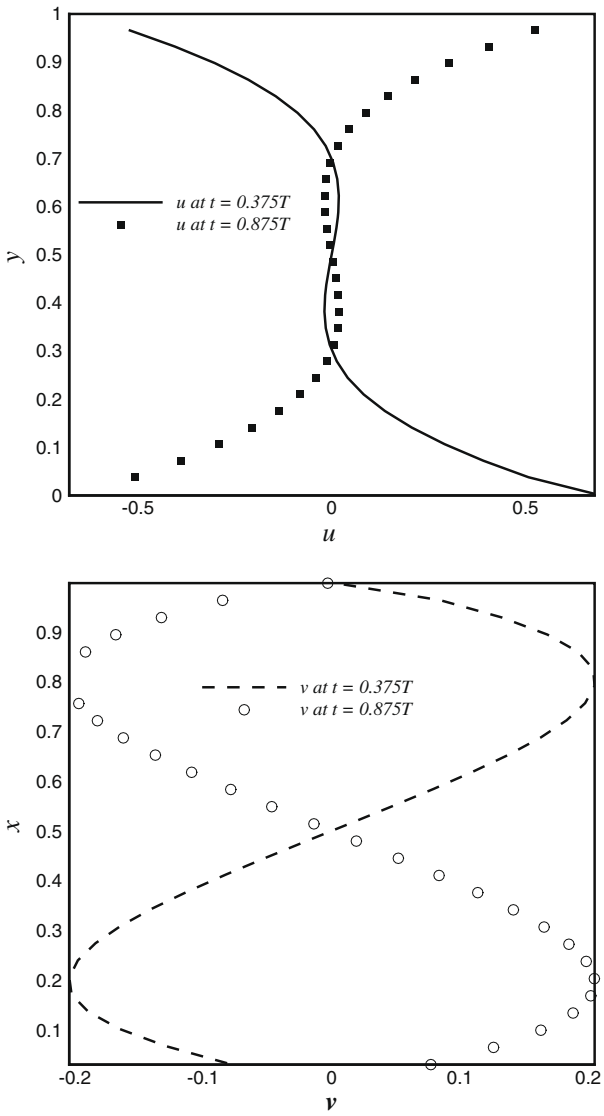

Fig. 7. Plot of velocity profile. u-Velocity along vertical centerline (upper) and v-velocity along horizontal centerline (lower).

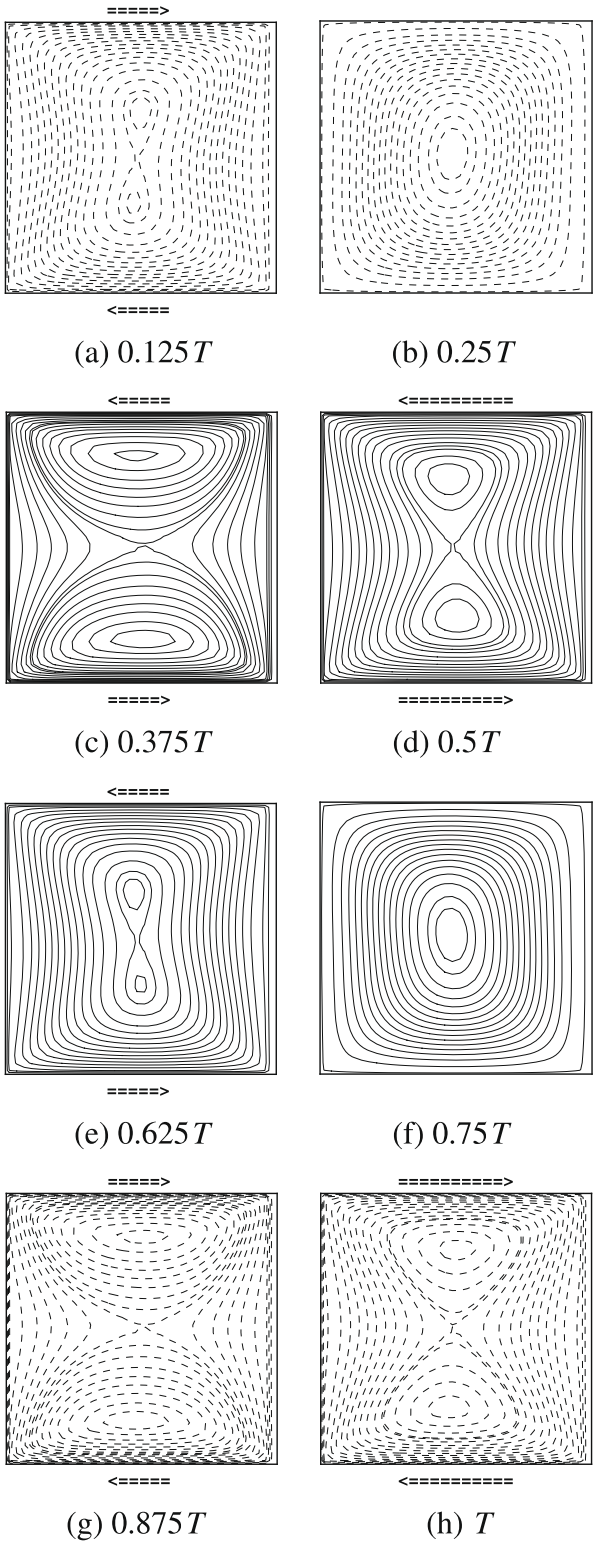

Fig. 8. Streamline contours during a period, Re = 10, $\varpi = 5$ (first mode).

time and the signs of the space coordinates and the velocity as shown in Figs. 5 and 7. We plot the time history of the u- and v-velocity at the center of the cavity (Fig. 5). It can be observed that the velocities change symmetrically after a half of period ($T = 2\pi = 6.283$). Similarly, the plot of u-velocity along the vertical centerline and v-velocity along the horizontal centerline at $t = 0.375T$ and $t = 0.875T$ indicate the symmetry operation between two parts of single cycle.

The simulations at the higher ϖ made a pair of vertical vortices bigger than the lower value of ϖ (Fig. 8). Nevertheless, the increment of ϖ up to 5 did not offer significant effect to change flow field. The flow patterns are stable and periodic with respect to two-dimensional perturbations and can still be categorized as the first mode.

3.1.2. A pair of swing vortices

The second mode is found at increasing Re and represented by Figs. 9 and 10. As the Re is increased, the flow will develop continuously. The two co-rotating eddies embedded in the main vortex (Fig. 9a and e). The size of the eddies is found smaller when the lid motion decelerated (Fig. 9b and f). These eddies merge together to form a single eddy in the middle of the cavity while the wall are emerged at the top and bottom lids. These wall eddies detach from the moving lids and grow inward (Fig. 9c and g). Eventually the middle eddy shrink and a pair of eddies is formed form the wall eddies (Fig. 9d and h). We could name these eddies as a pair of swing vortices since the condition at the first half of period was repeated with the oppo-

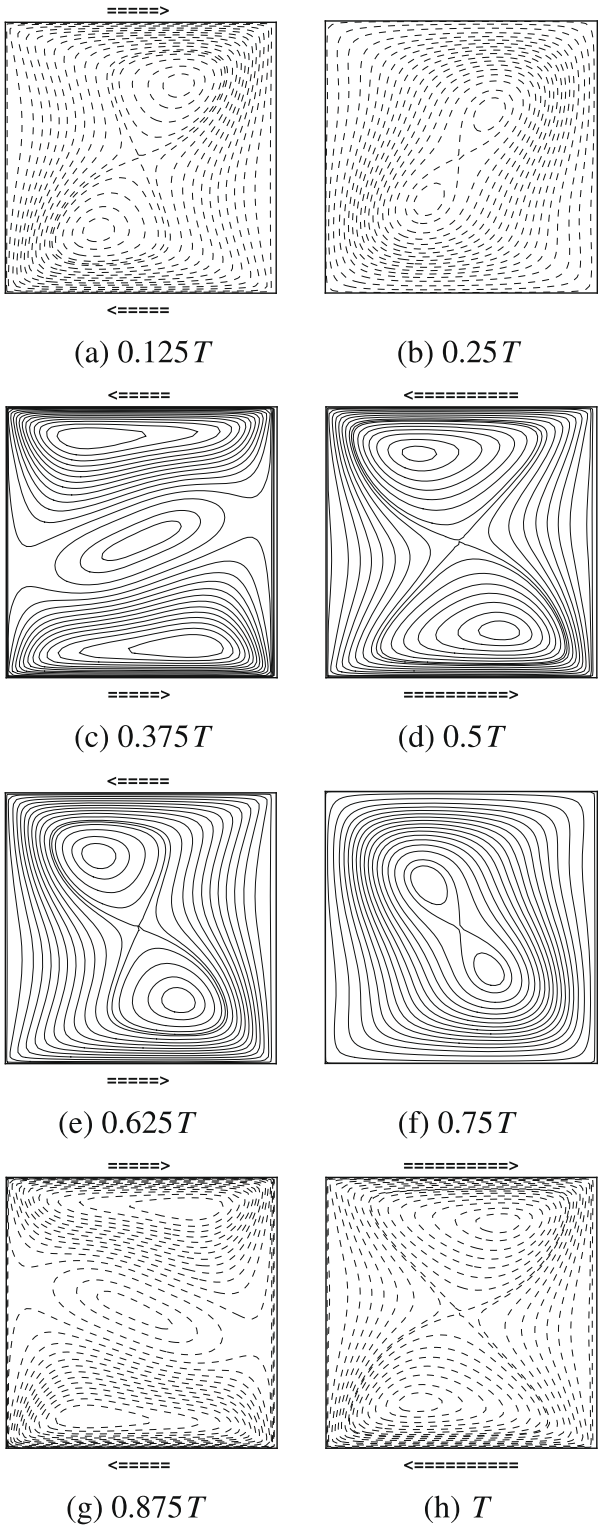

Fig. 9. Streamline contours during a period, Re = 100, $\varpi = 1$ (second mode).

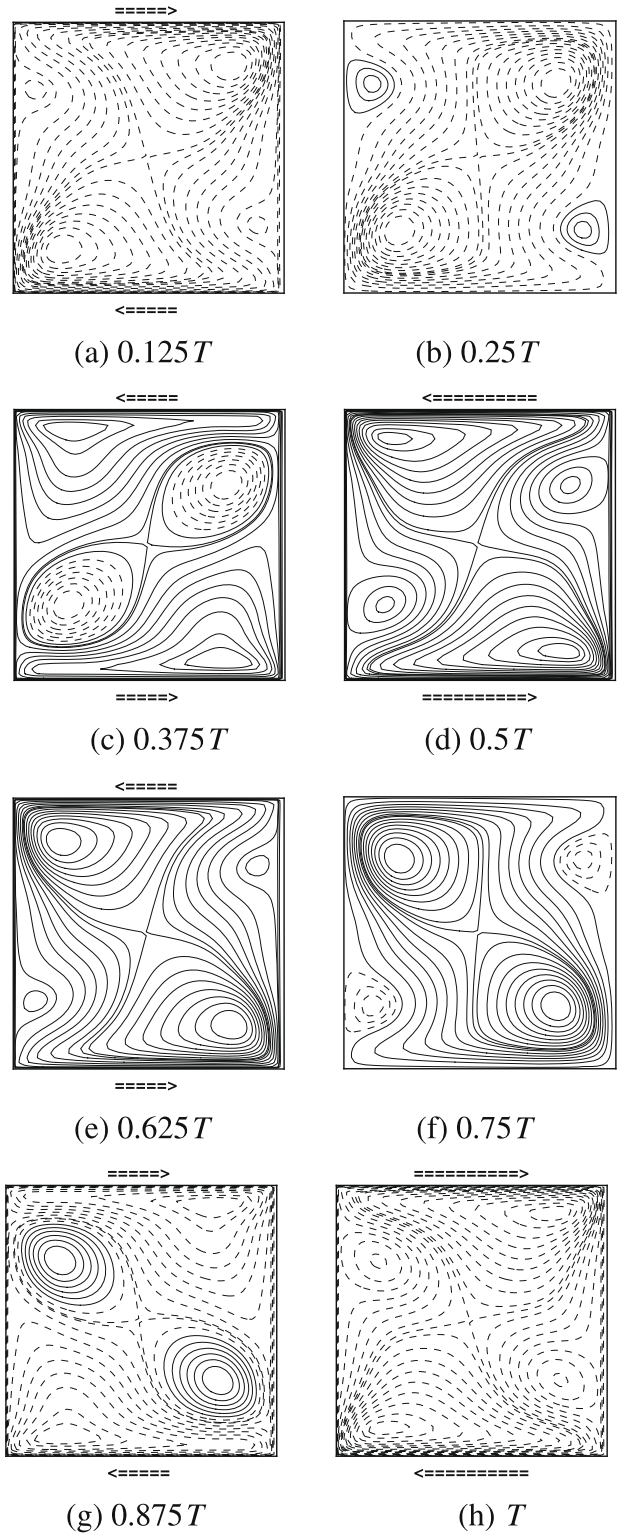

Fig. 10. Streamline contours during a period, Re = 500, $\varpi = 1$ (second mode).

site direction at the second half of period. The streamline patterns shown in Fig. 9a and e are taken as representation of this mode. The evolution of vortex formation of this mode differ form the first mode by detaching the eddy from the wall while in the first mode the vortex core is appeared in the bulk.

For high Reynolds numbers vortices are created near the downstream end of the moving lid. The acceleration by the moving lids will move the embedded eddies closer to the wall. As a consequence, a counter-rotating eddy is created in between. They detach from the moving lid and propagate along the stationary wall by following the lid motion (Fig. 10a, b, e and f). These eddies grow inward to form primary vortices when the lid motion changed to the opposite direction (Fig. 10c and g). At $t = 0.375T$ (Figs. 9 and 10c), the flow fields are divided to be

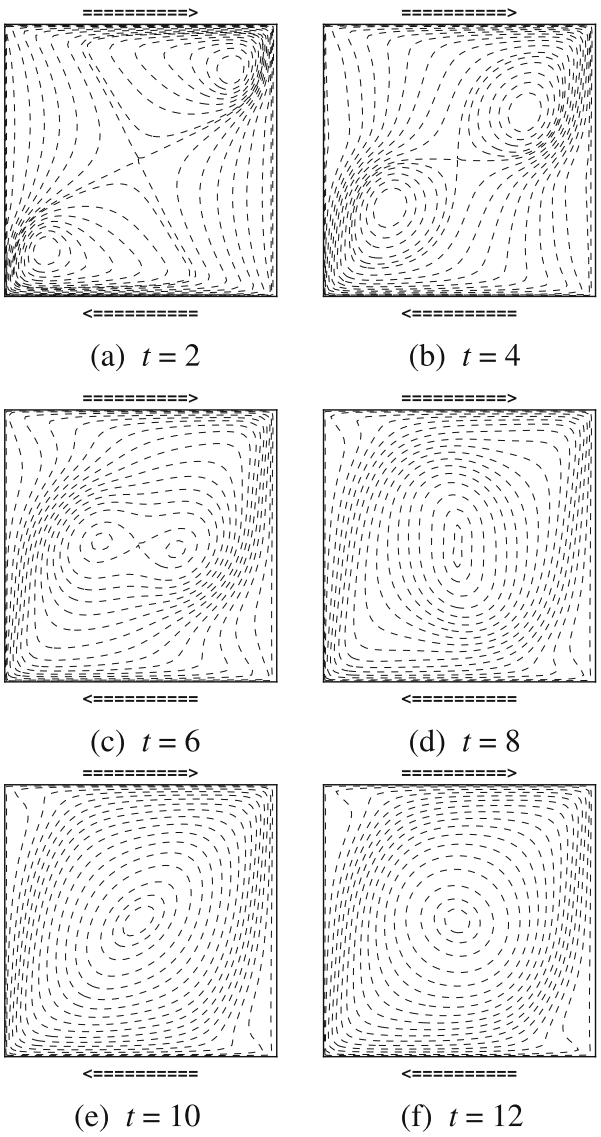

Fig. 11. The initial evolution of flow field inside a square cavity with double-sided constant lid motion at Re = 1000.

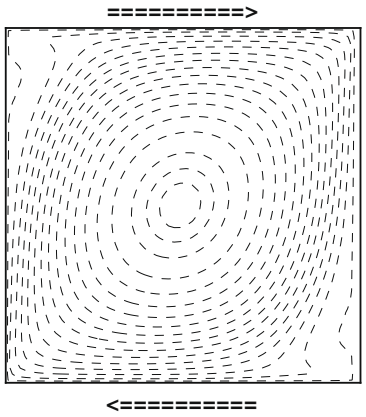

Fig. 12. The initial condition for Re = 1000, $\varpi = 1$.

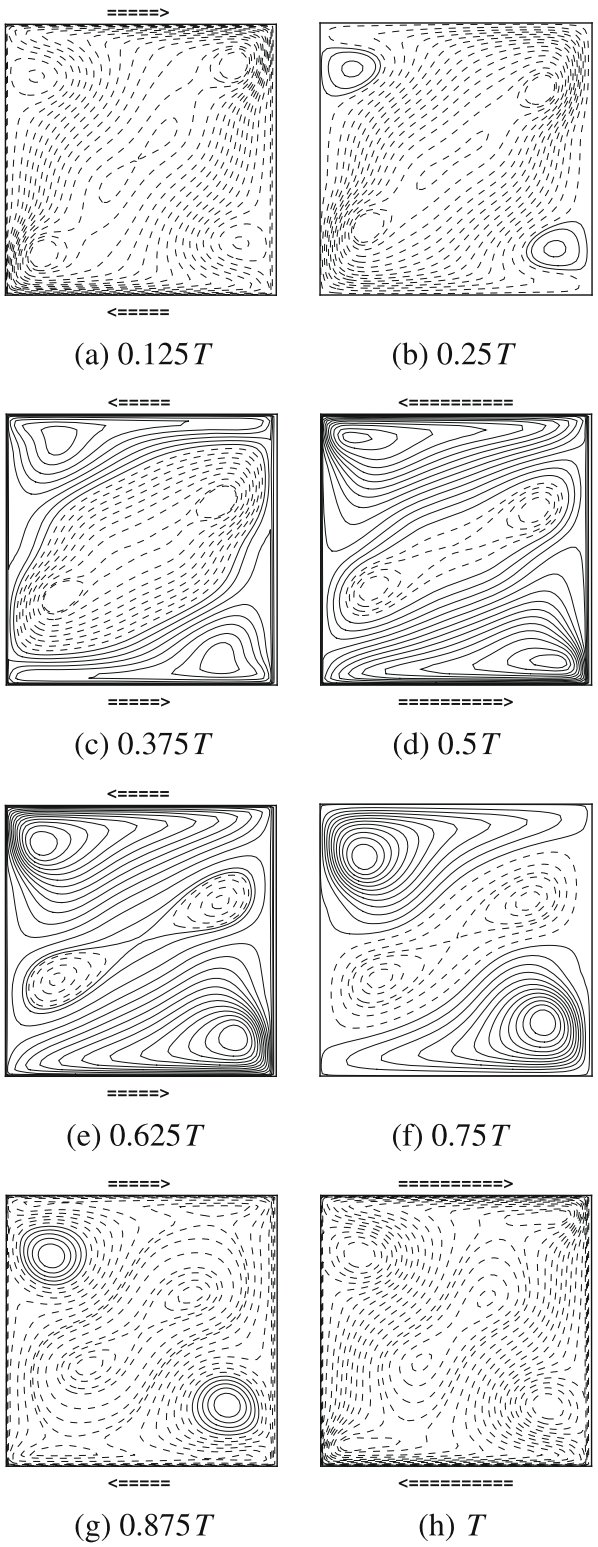

Fig. 13. Streamline contours during a period, Re = 1000, $\varpi = 1$ (third mode).

three regions. The vortices at the middle then broke out and replaced by the primary vortices coming from the top and bottom areas to form a pair of vortices with the saddle point at the center of the cavity (Figs. 9 and 10d).

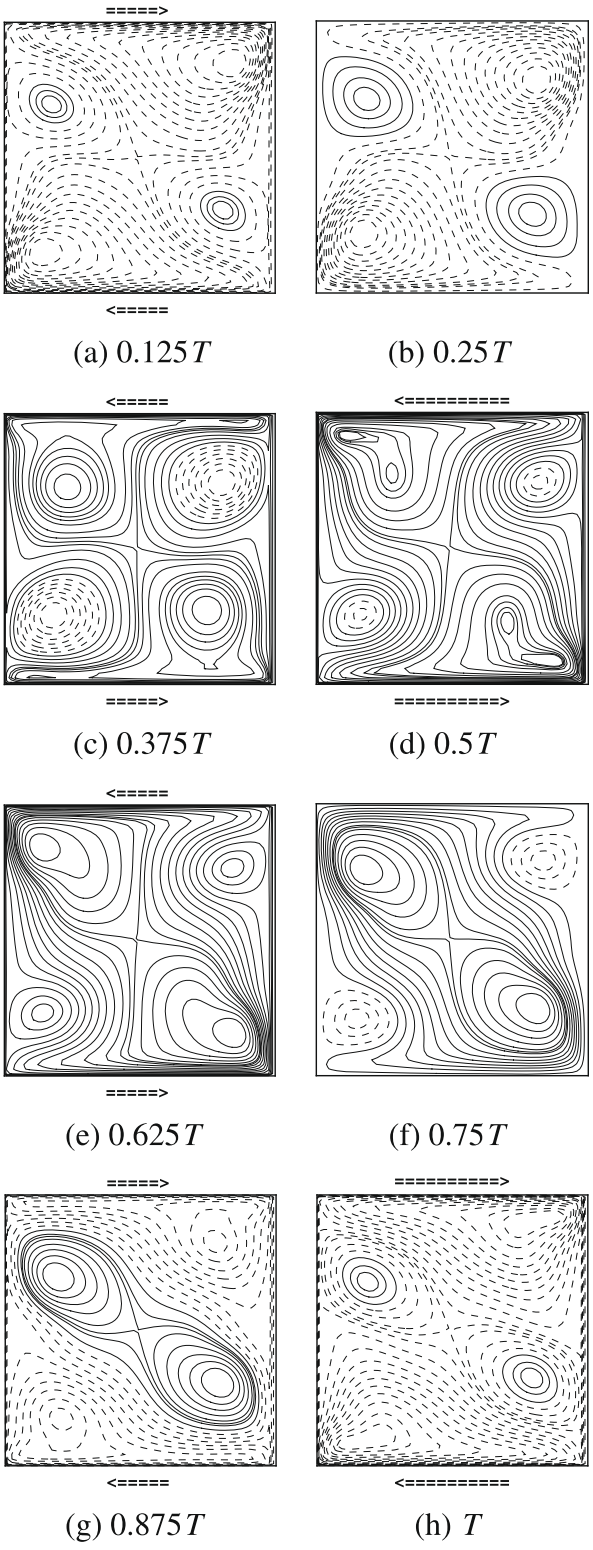

Fig. 14. Streamline contours during a period (the stirred initial condition), Re = 1000, $\varpi = 1$.

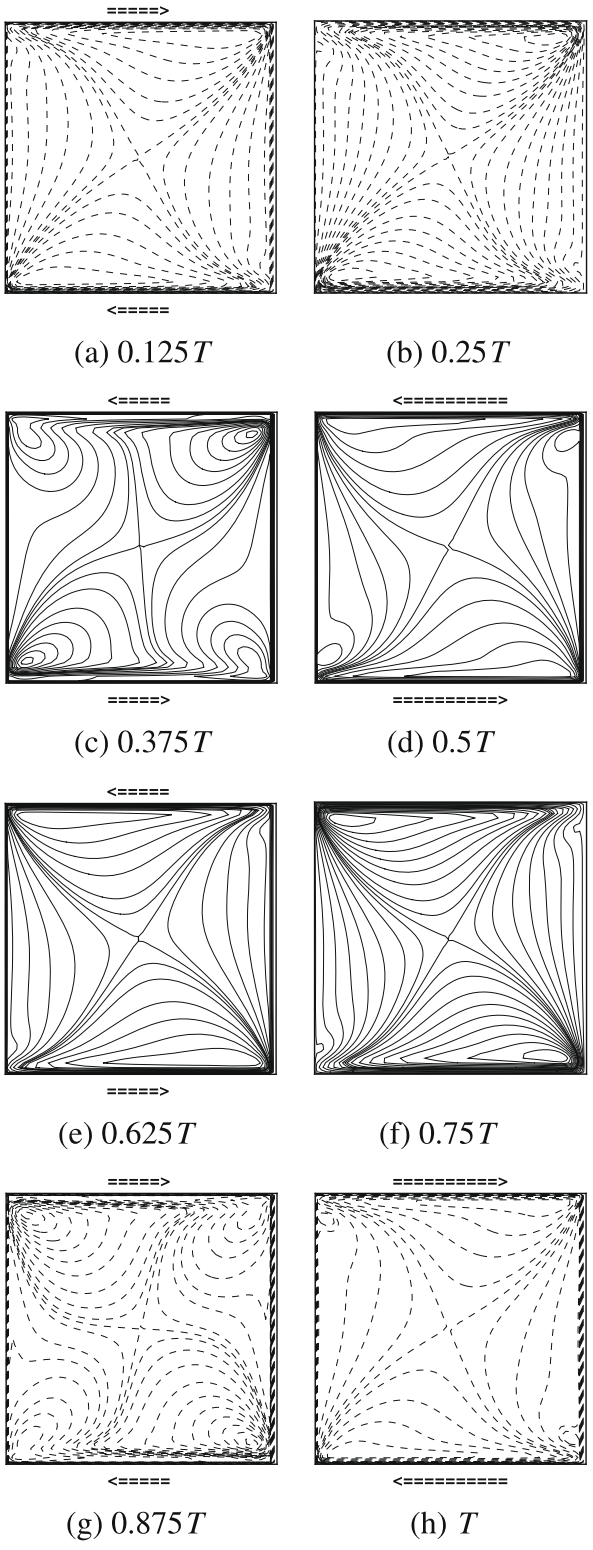

Fig. 15. Streamline contours during a period, Re = 1000, $\varpi = 5$ (fourth mode).

3.1.3. Diagonal-dominated vortices

Guermond et al. [20] investigated start-up flows in a three-dimensional rectangular driven cavity at Re = 1000. The initial evolution of this flow is studied up to the dimensionless time $t = 12$. The initial velocity field is zero in the entire cavity. As soon as the lid is set in upward motion, high shear stress develops along the cavity lid and generates a counter-clockwise-rotating primary eddy located close to the upper right corner. Furthermore, this primary eddy grows and moves towards the cavity center. As time increases, an additional clockwise-rotating secondary eddy appears at the mid-height of the upper wall. This wall-eddy grows and moves towards the upper left corner,

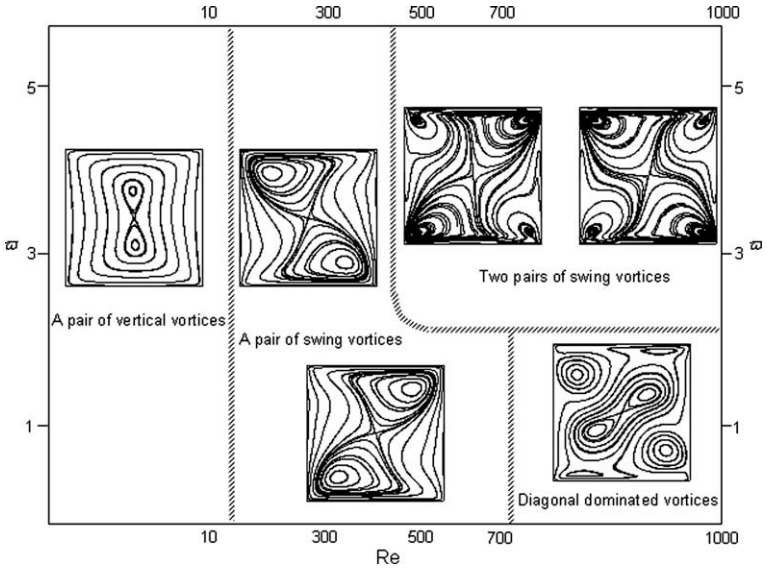

Fig. 16. Classification of flow fields.

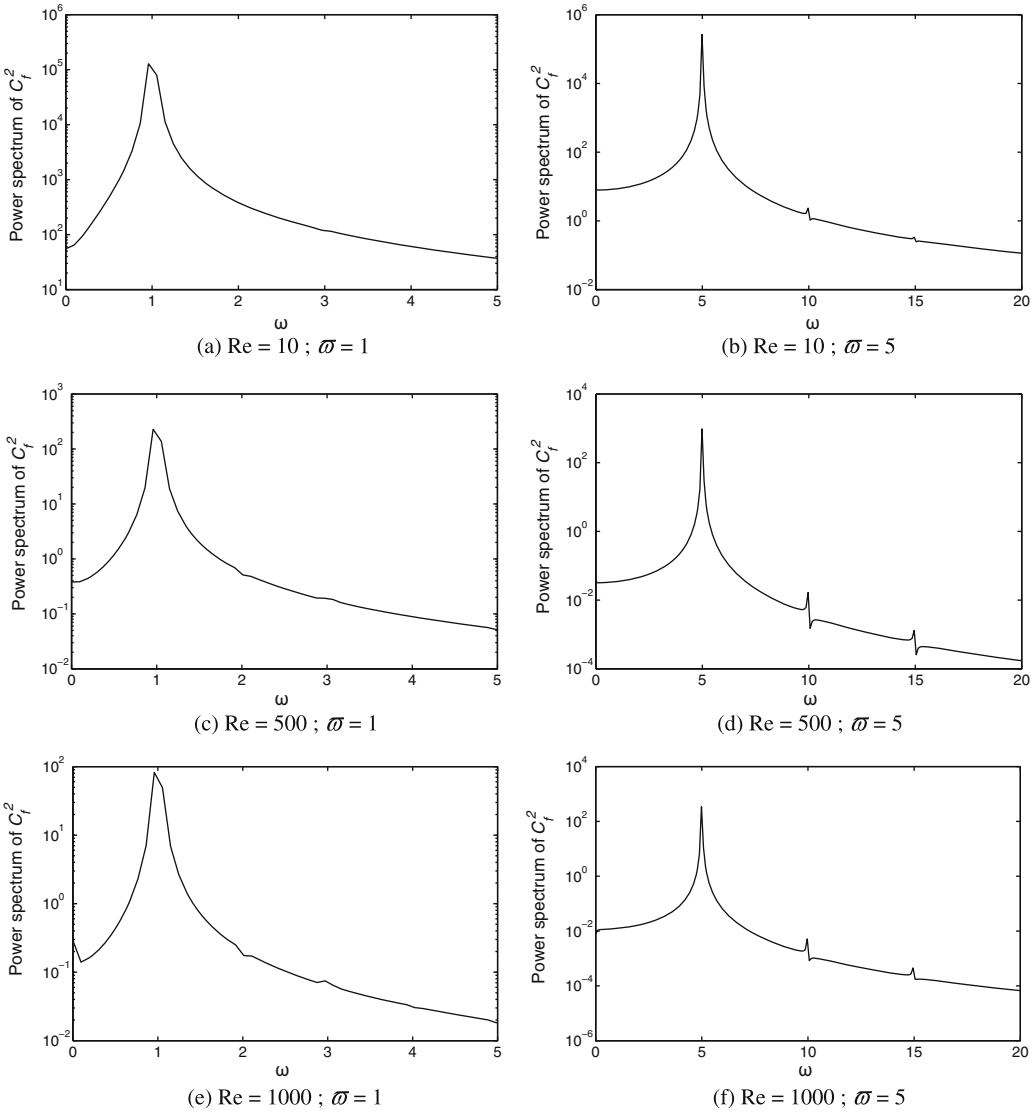

Fig. 17. Power spectrum of C_f.

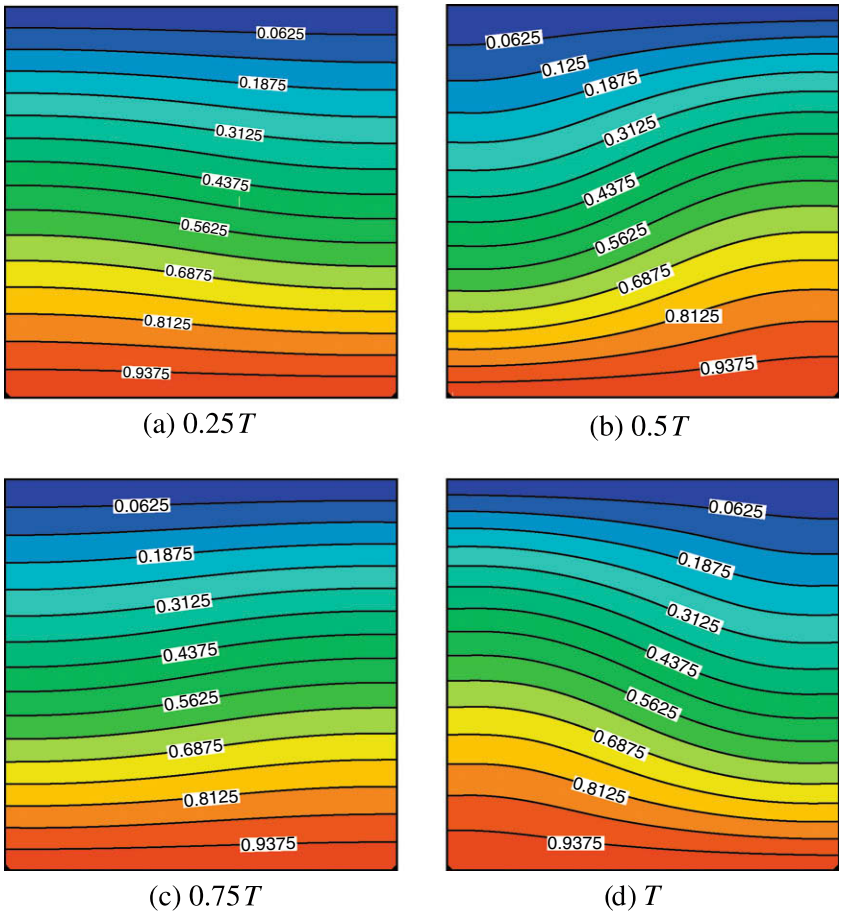

Fig. 18. Temperature contours during a period, Re = 10, $\varpi = 1$; (first mode).

and ultimately evolves to form the downstream secondary eddy in the established flow.

To compare our study with the work done by Guermond et al. [19], we performed the initial evolution for double-sided constant lid motion flow at Re = 1000. The temporal sequence of the streamline contours are shown in Fig. 11. At the beginning, the two clockwise-rotating eddies are formed at the bottom left corner and the upper right corner of the cavity (Fig. 11a). As time increases, these eddies move towards the center of the cavity and form a single primary eddy at the cavity center. During the dynamic evolution, this primary eddy changes until reach the steady solution as shown in Fig. 12. We use this steady solution as the initial condition for our simulation. Initially, it is apparent that the cavity is occupied by the primary diagonal eddy. This eddy is stretched and the dividing streamlines as well as the corner eddies are formed when the lids start to oscillate (Fig. 13). Even though the emerging corner eddies seem to affect the flow patterns during a period as occurs in the second mode, the diagonal eddies still exist and dominate the entire cavity. Furthermore we could call this case the diagonal-dominated vortices mode which falls for Re within the range of $700 \leqslant \mathrm{Re} \leqslant 1000$ and $\varpi = 1$.

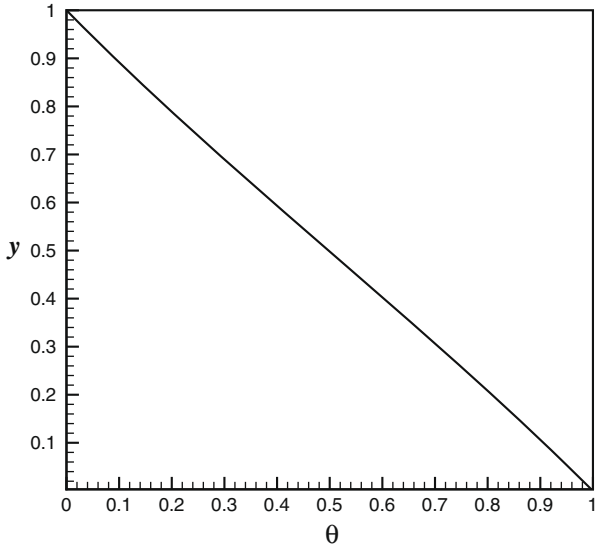

Fig. 19. Temperature profile along the y-direction at the mid-section of the cavity ($x = 0.5$), Re = 10, $\varpi = 1$; $t = 0.5T$ (first mode).

To further investigate the effect of the initial condition, we applied the stirred initial condition, i.e., the lids move oscillatory from the beginning while the fluids are at rest in such away that the diagonal-dominated vortices are not presented (Fig. 14). The evolution of vortex formation does not follow the second mode. The vortices occupy the entire cavity during the first half period are different from the second half of the period.

3.1.4. Two pairs of swing vortices

In the case of oscillatory Stokes flows evolving eddy structures in domains with sharp corners, Branicki and Moffatt [21] investigated the effect of the dimensionless frequency on the flow struc-

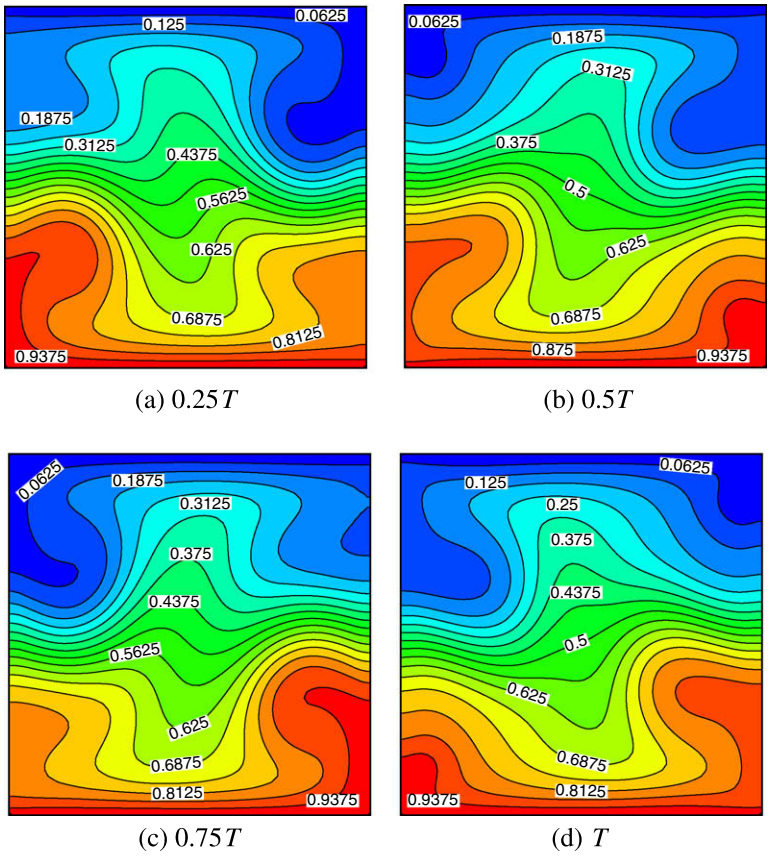

Fig. 20. Temperature contours during a period, Re = 500, $\varpi = 1$ (second mode).

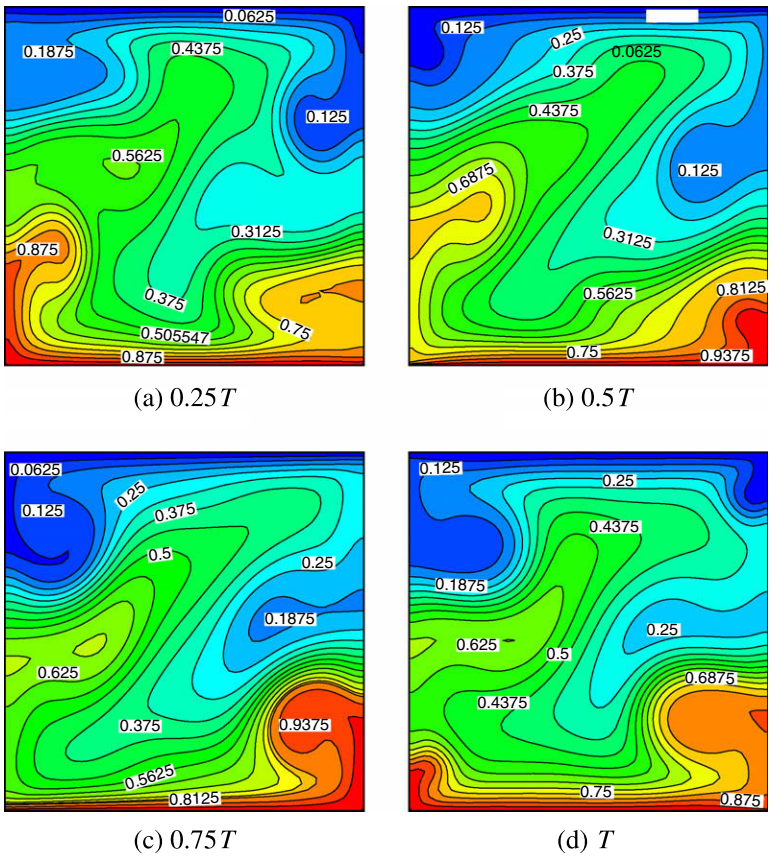

Fig. 21. Temperature contours during a period, Re = 1000, $\varpi = 1$ (third mode).

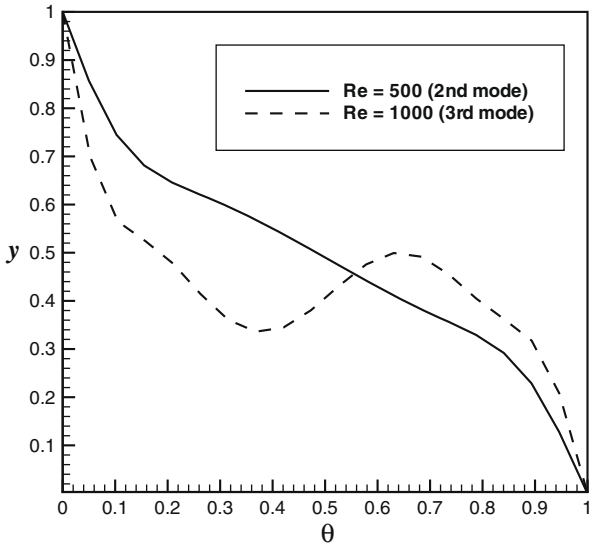

Fig. 22. Temperature profile along the y-direction at the mid-section of the cavity ($x = 0.5$), $\varpi = 1$; $t = 0.5T$ (second and third mode).

tures. For flow reversal in an oscillating square domain at low frequency, the eddies emerge at the four corners of the domain in opposite sense to the central eddy. These eddies grow inward and create a heteroclinic connection. As time increase, the connection shrinks and eventually annihilates the central eddy and the next flow reversal progress in a similar way. In contras to the flow reversal at low frequency, the corner eddies for higher frequency flow blend into Stokes layers and associated wall eddies which develop near the boundary. The flow reversal in the interior is realized through a series of global bifurcations involving wall eddies rather than the primary corner eddies.

Our simulation for higher Re and low ϖ (Re = 1000 and $\varpi = 1$) indicates similar flow behaviors with those of [20] as shown in Fig. 13. The corner eddies which are emerged at the downstream corners grow up when the direction of lid motion change (Fig. 13b–e), however, these corner eddies do not annihilate the diagonal central eddy. The dividing streamlines keep the central eddy rotates in clockwise direction while the corner eddies rotate in clockwise and counter-clockwise direction alternatively during a cycle. In contrast to the low ϖ where the emerging corner eddies expand into the interior and play a primary role in the flow reversal, the merging corner eddies for higher ϖ are ejected from the moving lids and travel along the walls from one corner to the others (Fig. 15c–d). These eddies eventually shrink into the Stokes boundary layers which dominate the flow structures near the walls. We observe that the saddle point always exist at the center of the cavity during a cycle. The dividing streamlines separate flow field in four region and avoid them transgressing each other.

Increase of oscillating frequency up to 5 changed the flow patterns become two pairs of swing vortices mode for medium and high Re as shown in Fig. 15. This mode is the fourth mode that has the similar behavior with the second mode. Two pairs of swing vortices existed and appeared alternatively after half of a period.

Finally, the modes of the flow patterns are presented in Fig. 16. The first mode is found at low Re for all values of ϖ given in this study. The second mode falls into large range of Re, $10 < \mathrm{Re} < 700$. For higher than 700, the third mode appears. The critical Re is found in the range of Re 290–320. Beyond this value, increase of ϖ creates the fourth mode. We notify that the classification of the flow patterns as mentioned above is taken from the solutions during a period at the 19th cycle based on steady lid motion as an initial condition. The stirred initial condition, as shown in Fig. 14, is not included in this classification.

The time histories of C_f along the top and bottom lids are analyzed using FFT technique. Fig. 17 reveals the power spectrum of C_f^2 at various Re and ϖ. There is a main appearing frequency at low Re (Fig. 17a). This main frequency is resulted from the motion of lids with $\varpi = 1$. Actually, for $\varpi = 1$ the flow is even harmonic. The peaks of the spectrum of C_f^2 are found weaker at higher Re (Fig. 17c and e). It indicated that C_f along lid surfaces is decreased as Re increased. The other harmonic frequencies are also found indistinctly at the higher Re (Fig. 17c and e). When ϖ increases up to 5, apart from the peak/main frequency at $\varpi = 5$, the other harmonic frequencies are found obviously at $\varpi = 10$ and $\varpi = 15$ (Fig. 17b, d and f). The second and

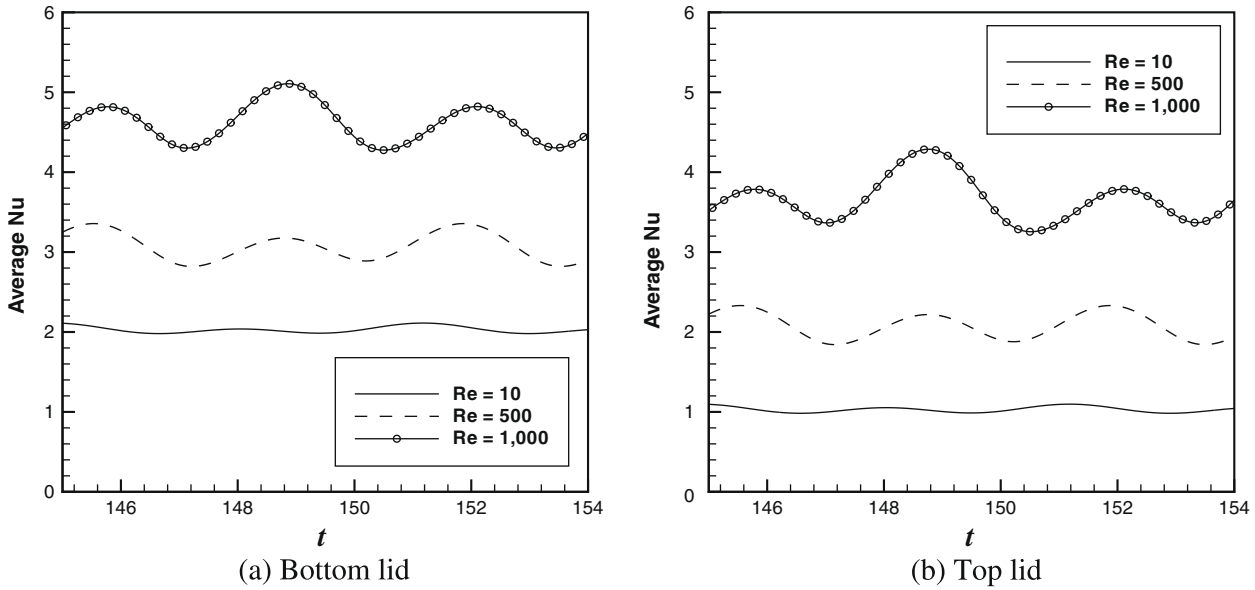

Fig. 23. Average Nusselt number at various Re, $\varpi = 1$.

the third harmonic frequencies just twice and three times the main frequency, respectively.

3.2. Isothermal profiles and average Nusselt numbers

At very low Reynolds number, the isothermal temperature contours during a period are shown in Fig. 18. It is observed that the isothermal contours were closed to the linear profile in which conduction is dominant. Plot of the linear temperature profile along the y-direction at the mid-section of the cavity ($x = 0.5$) indicates this phenomenon in Fig. 19. Flows at higher Re tend to increase the exerted shear force which creates higher momentum and energy transfer inside the cavity (Figs. 20 and 21). The flow fields for these cases are shown in Figs. 9 and 10, respectively. The temperature profiles were more complex than the previous one (Fig. 18) which was defined by the action of the primary and secondary vortices. The lower temperature regions along the x-direction were found at the locations wherein the vortices existed. The isotherms were accordingly clustered close to the hot bottom wall, which manifested the existence of high temperature gradient in the vertical direction. The profiles of temperature contours along the y-direction at the mid-section of the cavity (Fig. 22) give strong indication that convective heat transport becomes increasingly important compared to the diffusive heat transport. Furthermore, heat transport process becomes more effective in these cases which can be seen obviously from the plot of average Nusselt number, $\overline{Nu}$, on the bottom and top lid as shown in Fig. 23. Nu increased at the higher Re.

At small frequency of lid motion, ϖ, the oscillatory lid motion appreciably affected the bulk of the interior fluid. The augmentation

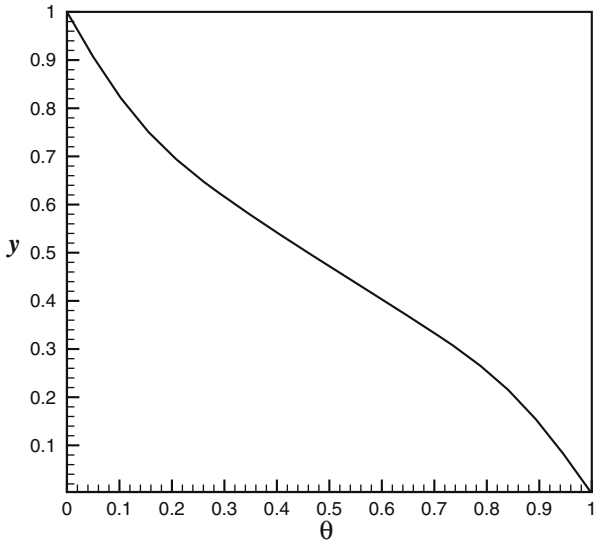

Fig. 25. Temperature profile along the y-direction at the mid-section of the cavity ($x = 0.5$), Re = 1000, $\varpi = 5$; $t = 0.5T$ (fourth mode).

of convective heat transfer was apparent at this condition. On the contrary, when the frequency was increased, the lid motion affected only the fluids confined in a shallow layer adjacent to the lids as shown in Fig. 15, i.e., the Stokes boundary layer is predominant in this case. This caused the weak interacting vertical structures of the fluid in the bulk of the interior region (Fig. 24) and leads to poor

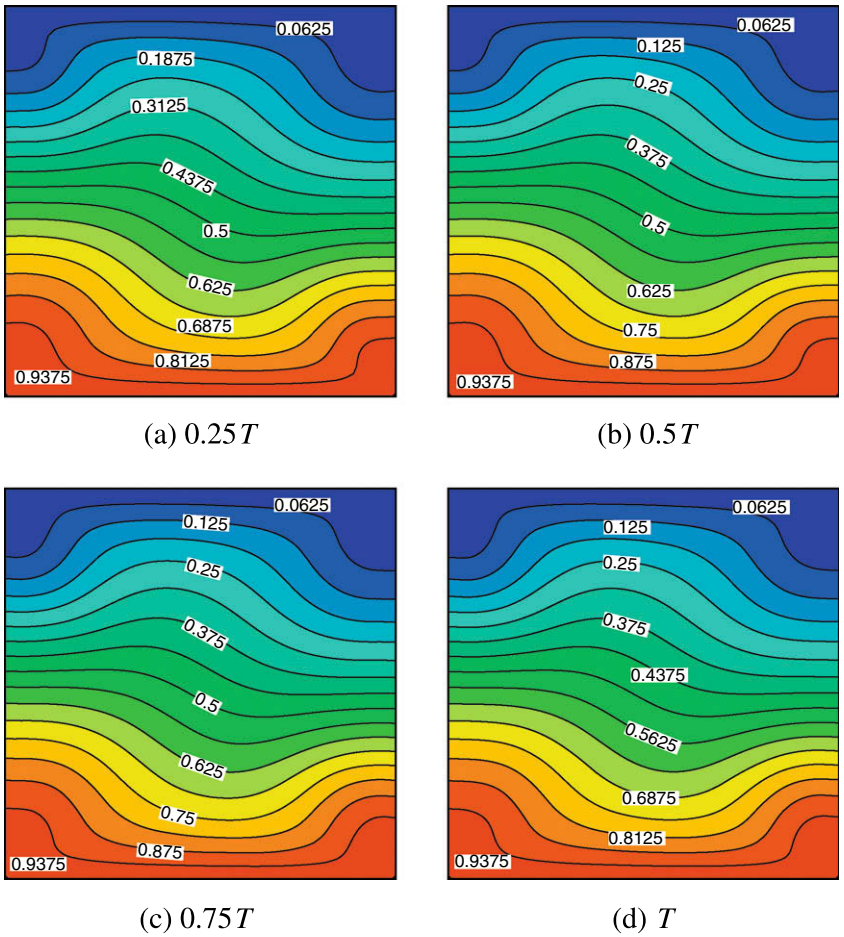

Fig. 24. Temperature contours during a period, Re = 1000, $\varpi = 5$ (fourth mode).

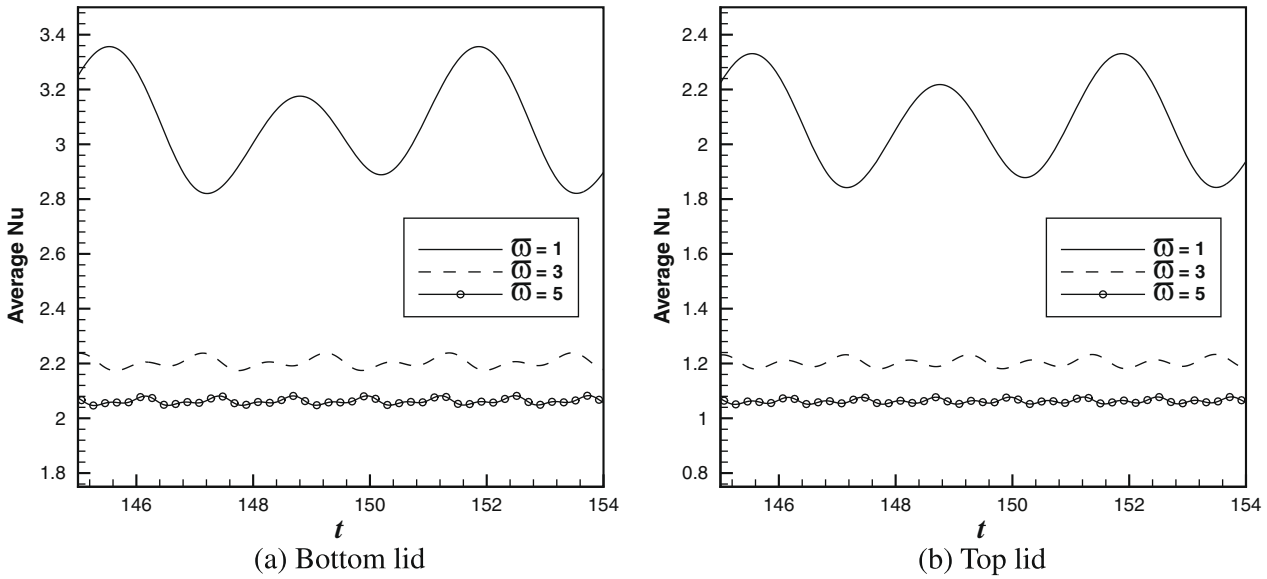

Fig. 26. Average Nusselt number at Re = 500, ϖ = 1, 3 and 5.

heat transfer. The temperature profile at the mid-section of the cavity along the *y*-direction, as shown in Fig. 25, tended toward a linear distribution that indicated existence of domination of conduction in this case. Clearly, this situation is reflected on the magnitude of predicted average Nusselt number at the bottom and top lids as shown in Fig. 26. Finally, we observe that the isothermal contours of all the modes, except for the third mode, have symmetric conditions during two parts of a single cycle. It is confirmed by the corresponding streamlines for each case at the same time period.

4. Conclusions

The flow and heat transfer are observed in a square cavity with double-sided oscillating lids in anti-phase. At simulations at Re up to 1000 and $\varpi = 1$, the flow patterns are classified into three modes, i.e., a pair of vertical vortices, a pair of swing vortices and diagonal-dominated vortices. As ϖ increased up to 5, the fourth mode, called as two pairs of swing vortices, was created at Re higher than 300. Increasing ϖ up to 5 at Reynolds number less than 300 gave variations on vortex sizes throughout the entire flow field. Nevertheless, it was not strong enough to change the mode of flow pattern. The flow patterns still can be categorized as the first mode and the second mode.

Heat transfer rates from the hot bottom lid to the cool top lid were affected by Re and ϖ. Higher heat transfer rates, indicated by Nu values, were found at higher Reynolds number flows due to the increase of fluid activities in the bulk of the interior fluids. On the contrary, heat transfer has become ineffective at high oscillating frequency since the motion of lids just affected the adjacent fluid layers. It is believed that an appropriate value of ϖ can enhance the overall heat transfer across the system boundaries due to the occurrence of resonance [10].

Acknowledgements

Funding from the university is gratefully acknowledged by the authors. The project is also supported by the National Science Council Taiwan under the Grant NSC 96-2221-E-001-098-MY3. Authors thank university computing center for providing the computing facility in the university cluster.

References

[1] M.M. Gupta, R.P. Manohar, Boundary approximations and accuracy in viscous flow computations, J. Comput. Phys. 31 (1979) 265–288.
[2] A.S. Benjamin, V.E. Denny, On the convergence of numerical solutions for 2-D flows in a cavity at large Re, J. Comput. Phys. 33 (1979) 340–358.
[3] U. Ghia, K.N. Ghia, C.T. Shin, High-Re solutions for incompressible flow using the Navier–Stokes equations and a multigrid method, J. Comput. Phys. 48 (1982) 387–411.
[4] R. Schreiber, H.B. Keller, Driven cavity flows by efficient numerical techniques, J. Comput. Phys. 49 (1983) 310–333.
[5] E. Barragy, G.F. Carey, Stream function-vorticity driven cavity solutions using *p* finite elements, Comput. Fluids 26 (1997) 453–468.
[6] M. Aydin, R.T. Fener, Boundary element analysis of driven cavity flow for low and moderate Reynolds numbers, Int. J. Numer. Methods Fluids 37 (2001) 45–64.
[7] Y.F. Peng, Y.H. Shiau, R.R. Hwang, Transition in a 2-D lid-driven cavity flow, Comput. Fluids 32 (2003) 337–352.
[8] E. Erturk, T.C. Corke, C. GÄokcÄol, Numerical solutions of 2-D steady incompressible driven cavity flow at high Reynolds numbers, Int. J. Numer. Methods Fluids 48 (2005) 747–774.
[9] W.H. Soh, J.W. Goodrich, Unsteady solution of incompressible Navier–Stokes equations, J. Comput. Phys. 79 (1988) 113–134.
[10] R. Iwatsu, J.M. Hyun, K. Kuwahara, Numerical simulation of flows driven by a torsionally- oscillating lid, J. Fluid Eng. 114 (1992) 143–151.
[11] T. Nishimura, K. Kunitsugu, Fluid mixing and mass transfer in two-dimensional cavities with time-periodic lid velocity, Int. J. Heat Fluid Flow 18 (1997) 497–506.
[12] S. Sriram, A.P. Deshpande, S. Pushpavanam, Analysis of spatiotemporal variations and flow structures in a periodically driven cavity, J. Fluid Eng. 128 (2006) 413–420.
[13] K.M. Khanafer, A.M. Al-Amiri, I. Pop, Numerical simulation of unsteady convection in a driven cavity using an externally exited sliding lid, Eur. J. Mech. B/Fluids 26 (2007) 669–687.
[14] H.C. Kuhlmann, M. Wanschura, H.J. Rath, Flow in two-sided lid-driven cavities: non-uniqueness, instabilities and cellular structures, J. Fluid Mech. 336 (1997) 267–299.
[15] S. Albensoeder, H.C. Kuhlmann, Three-dimensional instability of two counter-rotating vortices in a rectangular cavity driven by parallel wall motion, Eur. J. Mech. B/Fluids 21 (2002) 307–316.
[16] S. Albensoeder, H.C. Kuhlmann, Stability balloon for the double-lid-driven cavity flow, Phys. fluids 15 (2003) 2453–2456.
[17] W.-J. Luo, R.-J. Yang, Multiple fluid flow and heat transfer solutions in a two-sided lid-driven cavity, Int. J. Heat Mass Transfer 50 (2007) 2394–2405.
[18] C.W. Hirt, B.D. Nichols, N.C. Romero, SOLA – A Numerical Solution Algorithm for Transient Fluid Flows, Scientific Laboratory Report LA-5852, Los Alamos National Laboratory, NM, 1975.
[19] J. Jeong, F. Hussain, On the identification of a vortex, J. Fluid Mech. 285 (1995) 69.
[20] J.-L. Guermond, C. Migeon, G. Pineau, L. Quartapelle, Start-up flows in a three-dimensional cavity of aspect ratio 1:1:2 a Re = 1000, J. Fluid Mech. 450 (2002) 169–199.
[21] M. Branicki, H.K. Moffatt, Evolving eddy structures in oscillatory Stokes flows in domains with sharp corners, J. Fluid Mech. 551 (2006) 63–92.